Running Head: Impinging Spray Combustion in an Opposed-Piston Compression Ignition Engine

Spray Impingement and Combustion in a Model Opposed-Piston Compression Ignition Engine

Zhenyu Zhang[1], Peng Zhang[1,*] Zhenfeng Zhao[2]

1. Department of Mechanical Engineering, The Hong Kong Polytechnic University, Kowloon, Hong Kong

2. School of Mechanical Engineering, Beijing Institute of Technology, Beijing, PR. China

**Corresponding author, E-mail: pengzhang.zhang@polyu.edu.hk*

Abstract: *Sprays impingement and combustion in a model opposed-piston compression ignition (OPCI) engine was investigated experimentally and computationally. A recently proposed pressure-dependent droplet collision model was implemented in the KIVA-3V computer program for the RANS calculation, which was validated against the time-averaged experimental data for the cylinder pressure. Compared with the widely-used O'Rourke's model, the present model produces physically appraised predictions by accounting for the propensity of droplet bouncing upon collision at high engine pressures - a physical phenomenon overlooked in the previous models. The results show that droplet collisions can be promoted either by the impingement of the sprays from the oppositely placed three-nozzle fuel injectors under the condition of low engine speed and high load, or by the interaction of the sprays from each fuel injector in the presence of in-cylinder swirling flow. Motivated by fully utilizing the space of combustion chamber, a new spray layout possessing the S_2 symmetry was proposed and computationally investigated in the study. Compared with the Hofbauer's spray layout of the C_2 symmetry, the*

present layout tends to produce more distributed premixed fuel mass and hence results in a longer ignition delay time but a higher peak heat release rate.

Keywords: *Spray impingement; Spray combustion; OPCI; Droplet collision; KIVA-3V.*

1. Introduction

The development of opposed-piston two-stroke compression ignition (referred to as OPCI hereinafter) engines can be traced back to the coal-gas fueled opposed-piston engine developed by Witting in the 1850s (Pirault and Flint, 2010). Historically, OPCI engines were widely used in aircrafts, vehicles, and marines for their balanced performance and high efficiency. However, the increasingly stringent regulations on engine emissions since 1970s has restricted the development and application of OPCI engines. In recent years, there are rekindled interests in OPCI engines because the technological advances in emission control, including modern analytical tools, materials, high-pressure common rail fuel supply system and after-treatment system, have significantly mitigated the concerns about using OPCI engines.

Unlike the conventional four-stroke compression ignition (referred to as CCI hereinafter) engine, an OPCI engine has no cylinder head but two opposed pistons. So, fuel injectors in OPCI engine can only be mounted on the cylinder liner. In order to adequately utilize the in-cylinder air, two fuel injectors are oppositely arranged as such the sprays from each injector are apt to impinge with each other in the combustion chamber. Compared with the nearly non-interacting sprays in a CCI engine, the impinging sprays in the OPCI engine may substantially increase the collision frequency of fuel droplets. This could evoke an additional problem: the various

outcomes of binary droplet collision- coalescence, bouncing, and separation- can significantly affect the spray characteristics, particularly droplet size, velocity and distribution, and hence influence the subsequent fuel/air mixing and combustion (Law, 2010).

Many experimental studies have been conducted to identify collision outcomes for diverse liquids and unified understanding has been obtained. Three non-dimensional parameters, namely the collision Weber number, the size ratio and the impact parameter, are usually used to quantify the collision outcomes of binary droplets made of the same liquid. The Weber number measures the relative importance of the droplet inertia compared to the surface tension and can be defined as $We=\rho_l U^2 D_S/\sigma$ where ρ_l is the liquid density, D_S the diameter of the smaller droplet, σ the surface tension coefficient, and U the relative velocity of the colliding droplets. The size ratio, $\Delta=D_L/D_S$, is defined by the ratio of the diameter of the larger droplet D_L to that of the smaller one. The impact parameter is defined as $B=2X/(D_S+D_L)$, where X is the projection of the distance between the mass centers of the droplets in the direction normal to the relative velocity. A collision deviating from the head-on one, i.e. with $B=0$, has the impact parameter $0 < B \leq 1$. Earlier experimental studies have found that the colliding water droplets in atmospheric air either coalesce or separate. Motivated by understanding droplet collision in spray combustion, Jiang et al. (1992) and Qian and Law (1997) experimentally studied the droplet collision of n-alkanes and found that the droplets tend to bounce for a range of Weber number, beyond which they either coalesce or separate or splash at sufficiently large Weber numbers. Droplet bouncing was also observed for ethanol (Estrade et al., 1999) and for unequal-size droplets (Tang et al., 2012).

The emergence of droplet bouncing merits additional attentions, particularly under high ambient pressure condition. It has been experimentally observed that the droplet collision outcomes can be significantly affected by the ambient gas pressure and that droplet bouncing is promoted by increasing the pressure (Qian and Law, 1997). The underlying physics is that the increased inertia of the gas film separating the droplet surfaces hinders the rapid gas-film drainage that is required by droplet coalescence (Zhang and Law, 2011). In spite of the practical significance of droplet bouncing under elevated engine pressures, the only experimental study of Qian and Law (1997) addressed the problem up to 12 atm.

Modeling droplet collision is critical for predicting spray characteristics in the Lagrangian simulation of spray combustion in compression-ignition engines. The widely-used KIVA-3V computer program adopts the classic O'Rourke's (1981) droplet collision model, which was developed based on the earlier experimental observations on water droplets and predicts either droplet coalescence or droplet separation (Brazier-Smith et al., 1972). A number of modelling efforts were subsequently made to improve the over-simplified O'Rourke's model. In a brief summary, Tennison et al. (1998) and Aumann et al. (2002) extended the O'Rourke's model by taking into account of reflexive separation (for B=0). Estrade et al. (1999) introduced droplet bouncing into the O'Rourke's model and proposed a bouncing-coalescence criterion for hydrocarbon droplet collision. More sophisticated models have been developed to account for bouncing, coalescence, reflexive separation, stretching separation (for $0<B<1$), and fragmentation (i.e. splashing). A few excellent reviews have been given by Munnannur (2007), Munnannur and Reitz (2007) and Kim et al. (2009). However, none of these models considers

the influence of ambient pressure on the collision outcomes, specifically the tendency of the droplet bouncing at elevated pressures.

Motivated by simulating the impingement of non-reacting sprays in a quiescent high-pressure environment, where frequent droplet collision and bouncing are expected to occur, the authors (Zhang et al., 2016) proposed a practical droplet collision model by integrating a pressure-dependent factor to Estrade et al.'s (1999) model, accounting for the effect of ambient pressure on droplet collision outcomes. Regardless of the uncertainty of the factor due to the paucity and limitation of the available experimental data, their KIVA-3V simulations produce qualitatively satisfactory predictions to Chiba et al.'s (2000) impinging sprays at 10 atm and the authors' impinging sprays at 30 atm. Compared with the previous models without accounting for the propensity of droplet bouncing at elevated pressure, the authors' model predictions are in better agreement with the available experimental data about the shape, the penetration length, and the Sauter mean diameter (SMD) of the impinging sprays, and were found to be insensitive to the functional forms of the pressure-dependent factor.

A number of studies have been reported for the influence of spray impingement on OPCI engine performance. Hofbauer (2005) proposed an OPCI engine with opposed cylinders and found its advantages in power density and efficiency owing to its relatively high integration level and low heat loss. The influence of spray layouts on the engine performance was numerically studied by Hofbauer, employing the commercial software Star-CD with the O'Rourke's model. Franke et al. (2006) numerically and experimentally studied Hofbauer's spay layout in order to optimize the injector nozzle parameters, such as nozzle number and diameter, at different

in-cylinder swirl levels. Huo et al. (2015) numerically investigated the influence of combustion chamber structure on scavenging and combustion characteristics by using the commercial software CONVERGE. To improve the engine efficiency and reduce the emissions in the single-cylinder OPCI engine proposed by Regner et al. (2011), Naik et al. (2013) and Redon et al. (2014) optimized the scavenging process through experimental and numerical studies. Moreover, Venugopal et al. (2013) proposed a four-nozzle fuel injector and numerically studied the effects of spray angle by using CONVERGE with the O'Rourke's model.

In the present study, we aim to first extend our previous experimental and numerical study on impinging sprays, which was conducted in an initially quiescent, non-reacting chamber with constant volume and pressure, to the real OPCI engine conditions characterized by temporally-varying volume and pressure and with intensified swirling reacting flows. Additional objectives of the present study are to investigate the role of droplet bouncing in affecting the spray and combustion characteristics in a model OPCI engine developed by Zhao et al. (2014), and to computationally explore the possibly optimized spray layout for enhanced combustion performance. In the following text, we shall describe the experimental specifications of the adopted model OPCI engine in Section 2. The numerical methodology and the droplet collision modeling are summarized in Section 3, followed by the results and discussion, in Section 4.

2. Experimental Specifications of Model OPCI Engine

2.1 Engine Test System

To briefly illustrate the working principle of the model OPCI engine adopted in the present study, we showed the schematic of its gas exchange and fuel injection in Figure 1, where a Cartesian coordinate system is established so that the X-direction points inwardly to the paper. The OPCI engine employs a port-to-port uniflow scavenging system, which is regarded as an effective method to achieve high scavenging efficiency with low loss of fresh air. As shown in Figure 1 (a), the scavenging ports and exhaust ports are placed on the opposite sides of the cylinder, and the port opening and closing are controlled by the pistons moving along the Z-direction. At the end of the compression, as shown in Figure 1 (b), fuel sprays are injected, nearly along the Y-direction from the cylinder edge to the chamber center, and impinge with each other in the combustion chamber.

In the model OPCI engine, the engine bore is 100 mm, the stroke for each piston is 110 mm, and the displacement per cylinder is 3.4 liters. The exhaust port opens at 100° ATDC (after top dead center) and close at 113° BTDC (before top dead center); the intake port opens at 116° ATDC and close at 110° BTDC. In order to enhance the fuel/air mixing, intake ports are cut with a tangential of 20° to generate an in-cylinder swirl. The model engine can be stably operated with good repeatability up to the engine speed of 2000 rpm and the operation load of 50%. Operating the engine at higher speeds and larger loads was found to deteriorate the engine stability and repeatability and therefore deliberately avoided in the present experimental study

although it merits future improvement.

Figure-2 shows the schematic of the engine test system, in which the dashed and thick lines represent signal transmission lines and fuel oil pipes, respectively. To briefly describe the operation of the test system, the model OPCI engine (1) was coupled with an electrical dynamometer (2) to provide an engine load cell (3). Diesel fuel was stored in the fuel tank (4) and injected into the engine by the fuel injectors (5). Fuel consumption rate was determined by monitoring the weight of consumed fuel on an electronic scale (6). A Kistler 6056A water-cooled cylinder pressure transducer (7), which was installed on the first cylinder and coupled with a Kistler 2614B crank angle sensor (8), was used to determine the cylinder pressure as a function of crank angle (CA). The cylinder pressure data were collected with a time interval of 0.2° CA for 200 engine cycles. A Kistler 4005B pressure sensor (9) installed on the intake manifold and a Kistler 4049A pressure senor (10) installed on the exhaust manifold were used to measure the intake and exhaust pressures, respectively. In order to control the injection time and duration by the fuel oil driving pressure, a Kistler 4067A pressure senor (11) was installed on the high-pressure oil pipe between the injectors and the common rail (12). A resistance temperature detector temperature sensor PT100 (13) and a thermoelectric coupling sensor WRNK-191K (14) were used to measure the intake and exhaust temperatures, respectively. Signals from sensors (7)-(12) were processed by a Kistler 5011B charge amplifier (15) and collected by a data collection system (15).

The time, duration and mass of fuel injection, the intake and exhaust pressures, and the intake and exhaust temperatures were measured in the present experiment and used as input

parameters in the present numerical simulation. The measured cylinder pressure and the heat release rate accordingly estimated by using Krieger and Borman's (1967) method were used for validating the present numerical simulation. In order to reduce the estimation error, the average data of 200 cycles under steady engine operation conditions were used.

2.2 Cylinder-Pressure-Based Estimation for Heat Release Rate

As a summary of Krieger and Borman's (1967) method, applying the first law of thermodynamics to the engine combustion process yields

$$mC_v \frac{dT}{d\varphi} = \frac{dQ}{d\varphi} - \frac{dQ_w}{d\varphi} - P\frac{dV}{d\varphi} \quad (1)$$

where Q is the combustion heat release, Q_w the heat loss across the cylinder wall, W the work done by the engine piston, T the average gas temperature, P the experimentally determined engine pressure, V the cylinder volume, and φ the crank angle. By differentiating the ideal gas law, □□ = □□□, with respect to φ, we have

$$\frac{dT}{d\varphi} = \frac{1}{mR}\left(P\frac{dV}{d\varphi} + V\frac{dP}{d\varphi}\right) \quad (2)$$

Combining the above two equations, we have

$$\frac{dQ}{d\varphi} = \frac{dQ_w}{d\varphi} + \frac{\lambda}{\lambda - 1} P \frac{dV}{d\varphi} + \frac{\lambda}{\lambda - 1} V \frac{dP}{d\varphi} \tag{3}$$

where $\lambda = 1.37$ is the ratio of specific heats for the diesel combustion gas mixture.

The heat loss from the combustion chamber is mainly attributed to the convective heat transfer, which is estimated by

$$\frac{dQ_w}{d\varphi} = \frac{1}{6n} \sum_{i=1}^{2} a_i \cdot A_i (T - T_{wi}) \tag{4}$$

where n is the engine speed (in rpm), A_i the surface area, T_{wi} the wall temperature with $i = 1$ indicating the piston and $i = 2$ the cylinder liner. a_i $(i = 1,2)$ are the convection heat transfer coefficients estimated by

$$a_i = 820 P^{0.8} \cdot T^{-0.53} \cdot D^{-0.2} \times [C_1 C_m + C_2 \frac{T_a V_s}{P_a V_a} (P - P_0)]^{0.8} \tag{5}$$

where $C_1 = 2.28$ and $C_2 = 3.24 \times 10^{-3}$ is the constant, C_m the piston mean velocity (m/s), D the bore equal to 100 mm. P_a, T_a, V_a are the pressure, the temperature and the cylinder volume at the beginning of the compression.

2.3 Spray Layout of Model OPCI Engine

As has been discussed in the Introduction, the spray layout has a significant impact on the

OPCI engine performance. For example, Hofbauer (2005) and Franke et al. (2006) numerically studied a model OPCI engine with different spray layouts and found that three nozzles mounted on each injector results in optimal mixing performance. Venugopal et al. (2013) numerically studied the effect of spray angle on combustion and found that high temperature region and NOx emission can be significantly reduced by spray angle optimization. The schematic of the spray layouts considered in the present study is shown in Figure 3. The spray layout that was used in the present experiment adopts Hofbauer's three-nozzle spray design but with specific spray angles, as shown in Figure 3(a). Figure 3(b) shows the prototypical Hofbauer's spray layout with variable spray angles. Figure 3(c) shows a new spray layout design that was only used in the present simulation for spray layout optimization.

The schematic of the projections of the Hofbauer's spray layout on the X=0, Z=0 and Y=0 planes are shown in Figure 3(b). Each injector consists of three independent nozzles, which are referred to as Nos. 1–3 for the left injector and Nos. 4–6 for the right one. The Hofbauer's layout possesses the C_2 symmetry so that No. 1 and No. 4 sprays (similarly, No. 2 and No. 5, and No. 3 and No. 6) can interchange their positions by rotating for 180° with respect to the Z=0 axis. It should be noted that No. 2 and No. 5 sprays are on the Z=0 plane, and No. 1 and No. 3 sprays (Similarly, No. 4 and No. 6 sprays) are symmetrical with respect to the Y-axis. Owing to these symmetries, three angles can be used to completely determine the spatial positions and orientations of these sprays in the Hofbauer's layout. Specifically, α is defined as the angle between No. 1 (or Nos. 3, 4, 6) spray and the Y-axis on the Z=0 plane; β is defined as the angle between No. 2 (or No. 5) spray and the Y-axis on the Z=0 plane; γ is defined as the angle between No.1 (or Nos. 3, 4, 6) and the X-axis on the Y=0 plane.

In the present experiment, we adopted a slight variant of the Hofbauer's spray layout, as shown in Figure 3(a). It is seen that the C_2 symmetry is retained, No. 2 and No. 5 sprays are still on the Z=0 plane, but the symmetry between No. 1 and No.3 (also No. 4 and No. 6) is deliberately removed. As the representative case used in the present experiment for validating the simulation, the angles between Nos. 1-3 and the Y-axis are 45°, 5° and 30°, respectively; the angle between No.1 (or No. 4) and the X-axis on the Y=0 is 3°.

It is noted that the in-plane design of the Hofbauer-type layout for No. 2 and No. 5 sprays may promote the impingement of the sprays, it however does not fully utilize the space in the combustion chamber and therefore may result in locally high fuel concentration and incomplete combustion. Based on the consideration, we proposed a new spray layout for the present numerical study as shown in Figure 3 (c). This layout possesses the S_2 symmetry so that the No. 1 and No. 4 sprays (similarly, No. 2 and No. 5; No. 3 and No. 6) can interchange by a rotation of 180° with respect to the Z=0 axis followed by a mirror reflection with respect to the Z=0 plane. On the Z=0 plane, the symmetry between No. 1 and No.3 and that between No. 4 and No. 6 with respect to the Y-axis are retained as that in the Hofbauer's layout. Consequently, the same three angles, namely α, β and γ, can be defined to completely determine the spatial position of these sprays in this layout.

3. Numerical Methodology

The present Reynolds Average Navier-Stokes (RANS) calculation of the model OPCI engine with spray impingement and combustion was carried out by using the KIVA-3V

computer program. It is noted that there is an increasing trend in applying large eddy simulation (LES) to engine combustion, but LES was not employed in the present study. As discussed in Section 2, all of the present experimental data are time-averaged pressures, such as the average cylinder pressure, the average intake pressure, and the average exhaust pressure. Owing to the lack of time-resolved experimental measurements, which are technically challenging albeit merited for future study, it is less meaningful to either compare time-averaged LES results with experimental data or compare LES and RANS calculation in the present study.

It is recognized that the OPCI engine combustion involves complex multi-phase flow, heat and mass transfer, and chemical reaction. The present study has no intention to employ and compare the sophisticated models for droplet breakup, evaporation, mixing and turbulent combustion. Instead, the RANS calculations with the standard numerical schemes and models implemented in KIVA-3V were used to facilitate the comparison of droplet collision models with and without considering the ambient pressure effects.

In the present RNAS calculation, we adopted the standard k-ε model for turbulence modelling, the SIMPLEC method for velocity-pressure coupling. Fuel was injected into the combustion chamber in the form of liquid droplets of the nozzle size and the injection pressure is 160 MPa. The injection time and duration were determined from the experiment as discussed in the preceding Section. The discharge coefficient of injector nozzle in the present study is 0.7, which was used to estimate the mass flow rate of the fuel injection. To simulate a complete engine cycle, the calculations started at -180° ATDC and ended at 180° ATDC.

The TAB model (O'Rourke and Amsden, 1987) and the Spalding model (Launder and Spalding, 1972) were used to account for the droplet breakup and droplet evaporation. The Arrhenius law was used to calculate chemical reaction rate constants. The details of these models are expatiated in the manual of KIVA-3V (Amsden, 1997). Although it is well known that the TAB model tends to predict excessive atomization for high injection pressures, it was still used in the present study to not distract the focus of the present study by employing and comparing the more sophisticated models for droplet breakup and evaporation and for turbulent flows, which have been extensively studied in the literature (Heywood, 1988, Sirignano, 1999).

The pressure-dependent droplet collision model adopted in present study has been sufficiently discussed and validated in our previous study (Zhang et al., 2016) and will be briefly described here. To account for the experimental observation of Qian and Law (1997) that droplet bouncing is promoted by increasing the ambient pressure, a pressure-dependent factor g(p) was added to the widely used bouncing criterion of Estrade et al.'s as

$$We < We_{cr}(p, \Delta, B) = g(p) \cdot We_{cr}(1,1,0) \frac{\Delta(1+\Delta^2)(4\Theta'-12)}{2.8\chi_1\{\cos[\sin^{-1}(B)]\}^2} \quad (6)$$

where $We_{cr}(p, \Delta, B)$ is the bouncing-coalescence transition Weber number at various p, Δ and B; $We_{cr}(1,1,0)$ is the number for head-on collision at p=1 (in atm), Δ=1, and B=0. The pressure-dependent factor was fitted in three power-law formula, namely $g(p)= ap^{\beta}+b$ with β=0.5, 1.0 and 2.0, by using the experimental data of (Qian and Law, 1997). It was found that

the three fitting formulas make insignificant difference in the simulations of impinging sprays up to 30 atm. Consequently, the linear fitting $g(p)= 0.25p+0.75$ was used in the present simulation. In the Estrade et al.'s model, the shape factor $\Theta'=3.351$ and $\chi_1=1-0.25(1+\tau)(2-\tau)^2$ if $(r_1+r_2)(1-B)>r_1$, otherwise $\chi_1=0.25(3-\tau)\tau^2$, where $\tau=(1-B)(1+\Delta)$. Furthermore, it should be realized that reflective separation and stretching separation can be substantially suppressed in a high ambient pressure environment, where droplet bouncing and coalescence are the dominant outcomes of droplet collision. Consequently, the droplet collision model adopted in the present study does not account for those collision outcomes occurring usually at very high Weber numbers.

To illustrate the difference between O'Rourke's and Zhang et al.'s models, Figure 4 compares the regime nomograms of droplet collision, based on which the two models were established. As mentioned in Section 1, the O'Rourke's model accounts for coalescence and off-center separation (a.k.a stretching separation) because bouncing is absent in water droplet collision at atmospheric pressure. Droplet bouncing is nevertheless considered as the primary collision outcome under higher ambient pressure (Qian and Law, 1997, Zhang et al., 2016) because the bouncing-coalescence boundary right shifts to higher Weber numbers on the nomogram with increasing the pressure. As a result, droplet collision with the same Weber number tends to result in coalescence in O'Rourke's model but bouncing in Zhang et al.'s model. Significantly different model predictions to the droplet size distribution are expected to be seen in the KIVA-3V simulation with the two models.

Full-scale three-dimensional mesh with intake ports and exhaust ports was generated by ICEM CFD. Figure 5 shows an example in which the total number of mesh cells at BDC (bottom dead center) is 200615 and that at TDC is 32748. Recognizing that in-cylinder gas motion and droplet collision probability predicted in KIVA-3V are sensitive to mesh cell size, we conducted a mesh-dependence test for the spray impingement and combustion in the model OPCI engine with the engine speed of 1500 rpm and under 50% load. The predicted cylinder pressure for four different meshes from the coarsest one with 159552 cells to the finest one with 255742 cells are shown in Figure 6. It is seen that the four meshes produce almost identical prediction regardless of the slight undershooting of the coarsest mesh. As a result, the intermediate mesh with 200615 cells was adopted in the following simulations as a balance of computational time and calculation accuracy.

4. Results and Discussion

4.1 Experimental Validation of Numerical Simulation

To validate the present numerical methodology and droplet collision models, we conducted the model OPCI engine experimental test at the engine speeds of both 1500 rpm and 2000 rpm, and under 50% load. The experimental in-cylinder pressure, estimated heat release rate and the numerical results employing Zhang et al.'s droplet collision model are shown in Figure 7 for comparison. It is noted that the intake temperature was 325 K, and the intake pressure was 1.2 bar for 1500 rpm and 1.6 bar for 2000 rpm. At the engine speed of 1500 rpm, the predicted cylinder pressures show very good agreement with the measured data within the entire engine

cycle, indicating that the present simulation captures accurately not only the pressure variation due to the piston motion before ignition but also the pressure variation due to the combustion heat release. The peak value of the predicted heat release rates is slightly higher than the estimated heat release rate by using the Krieger and Borman's (1967) approximation method. It should be noted that the estimated heat release rate based on the measured cylinder pressure is merely an approximate approach to characterize the engine combustion performance. In addition, the calculated heat release rates are also affected by the uncertainties from the models for fuel vaporization and combustion chemistry. Therefore, further analysis of the small discrepancy is inapplicable in the present study although it merits future work. At the engine speed of 2000 rpm, the good agreement between the simulation and experiment is still held for the in-cylinder pressure. The predicted heat release rate overshoots the estimated one after ignition, possibly because the mixing combustion model adopted by the present simulation overestimates the chemical reaction rates.

The detailed discussion and validation of the present droplet collision model has been given in the previous study (Zhang et al., 2016) for nonreacting spray impingement, where the O'Rourke's model is compared and analyzed for its deficiency at elevated pressure in overestimating droplet sizes after collision. For a brief summary, in order to validate the present droplet collision model at elevated pressures, the authors calculated Maruyama et al.'s (2001) experiments on the free and impinging sprays in a constant-volume chamber filled with nitrogen of 10 atm. The calculations based on the KIVA-3V program with the Zhang et al.'s droplet collision model show good agreement with the experimental results on various spray characteristics, such as the shape, the penetration length and the Sauter mean diameter (SMD).

To further validate the present droplet collision model at higher pressures, time-evolving multiple impinging sprays were experimentally and numerically studied at 30 atm. Again, the Zhang et al.'s droplet collision model not only qualitatively captures the spray development by reproducing the experimental time-resolved shadowgraph images but also quantitatively predicts the spray spreading characteristics, which is quantified by using the gray-level analysis to the experimental shadowgraph images. These qualitatively satisfactory predictions of the Zhang et al.'s model stress the significance of the physical phenomenon that colliding droplets at high gas pressures tend to bounce back and however is not accounted for in the previous models.

To further compare these two models under the combustion condition, the predicted physical quantities characterizing the spray impingement and combustion in the model OPCI engine are shown in Figure 8. Specifically, Figure 8 (a)-(c) shows the case at the engine speed of 1500 rpm and 50% load, which has been validated by the experimental data for the cylinder pressure and heat release rate. To extend the comparison to higher engine load, which was however not able to achieve in the present experiment, we show the case at the same engine speed but with 75% load, in Figure 8 (d)-(f). In this case, intake temperature was 325 K, intake pressure is 1.5 bar.

Figure-8 (a) and (d) show the evolution of the Sauter mean radius of all the droplets (SMR, on the left Y-axis) and the parcel number (N_p, on the right Y-axis) for different loads. For the case of 50% load as shown in Figure 8 (a), the SMR decreases rapidly after the fuel injection at -5° ATDC and then reaches a steady value of approximately 60 μm. The SMR predicted by the present model is slightly lower than that by the O'Rourke's model around -3° ATDC. For the

evolution of N_p, the O'Rourke's model predicts an approximate plateau of N_p for about 4° before N_p starts to decrease after the ignition at around 0.5° TDC. N_p precided by the present model, which has a peak value at around -3° ATDC, is higher than that by the O'Rourke's model before the ignition occurs. These observations can be understood by that the droplets injected into the high-pressure engine chamber tend to coalesce in the O'Rourke's model and therefore result in bigger droplet sizes and smaller N_p. With the engine load increases to 75% as shown in Figure 8 (d), the present model predicted significantly lower SMR and higher N_p, as the result of more fuel droplets are injected to the engine under such a high load and result in more collisions, which substantially augment the difference between the two model predictions.

To quantify the evaporation and mixing processes, we defined a time-dependent ratio A_d=$N_p(t)\mathrm{SMR}^2(t)/N_p(0)\mathrm{SMR}^2(0)$, where $N_p(0)$ and SMR(0) are the initial parcel number and SMR, as an indicator of total droplet surface area. Figure 8 (b) and (e) show the evolutions of A_d (on the left Y-axis) and premixed fuel mass (on the right Y-axis) at different loads. At the 50% load, there is no significant difference between the two model predictions for A_d and hence the premixed fuel mass, as the predicted SMR and N_p are close. Because A_d has a stronger dependence on SMR than N_p, the O'Rourke's model predicts slightly higher A_d around -3° ATDC due to the higher SMR while the smaller N_p. At the 75% load, the O'Rourke's model predicts substantially higher A_d and thus premixed fuel mass than the present model because of the significantly smaller SMR and larger N_p. By the same token, the present model however predicts significant higher A_d and hence higher premixed fuel mass after 1° ATDC, after when it predicts similar SMR but significant higher N_p than the O'Rourke's model.

Figure-8 (c) and (f) show the heat release rate (on the left Y-axis) and the cylinder pressure (on the right Y-axis) at different loads. SOI denotes the start of injection; EOI the end of injection. The ignition time (IT) is defined as the instant when 5% of total heat release has been obtained, and thus the time period between SOI and IT can be defined as the ignition delay time. It is noted that, SOI= -5° ATDC for both loads, while EOI=9° ATDC for 50% load and 12.5° ATDC for 75% load. It is well known that compression ignition in OPCI can be divided into two phases, namely the premixed phase and the diffusion phase (Regner et al., 2011, Naik et al., 2013, Venugopal et al., 2013). The premixed phase can be identified as the time duration between the IT to the time corresponding to the local minimum between two peak values on the heat release curve. It can be seen in Figure 8(c) that, there is no significant difference between the two models in predicting the cylinder pressure, the IT, and the heat release rate at the 50% load. For the 75% load, shown in Figure 8 (f), because of the smaller A_d and premixed fuel mass before 1° ATDC, the present model predicts a later ignition, compared with the O'Rourke's model. The higher peak heat release rate predicted by the present model, which in turn results in the higher cylinder pressure, can be again attributed to the significant higher premixed fuel mass accumulated after 1° ATDC.

4.2 Influence of In-cylinder Swirl on Spray and Combustion Characteristics

In the present OPCI model engine, the intake port was cut into an angle of 20° to generate in-cylinder swirl. In order to investigate the influence of the in-cylinder swirl on the spray

characteristics, we compared the evolution and interaction of the non-reacting sprays under non-swirl (i.e. intake port angle of 0°) and swirl (i.e. intake port angle of 20°) conditions, as shown in Figure 9. It should be noted that a working condition of 2000 rpm and 75% was used in this subsection in order to explore the spray and combustion characteristics under the more practical situations of the OPCI engine. The intake temperature was 325 K, intake pressure is 1.7 bar. In the non-swirl case, a manifest impingement between the No. 2 and 5 sprays can be observed at around 4° ATDC, predicted by both models. With the presence of the in-cylinder swirl, the swirling flow exerts high tangential forces on the droplet parcels and hence significant spray deflection was observed. The most influential consequence of such spray deflection is that the inter-injector impingement between the sprays from the bottom injector (i.e. No.1-3 sprays) and those from the upper injector (i.e. No.4-6 sprays) was suppressed. Instead, the intra-injector interactions emerge between the No.1 and No.2 sprays from the bottom injector, and between No. 4 and No.5 sprays.

Apparently, both the inter-injector and intra-injector spray impingement is able to enhance droplet collision and hence necessitate its proper modeling in the engine simulation. Figure 10 shows the quantitative comparison of the Zhang et al.'s and O'Rourke's models for predicting the non-reacting spray impingement shown in Figure 9. In the non-swirl case where frequent droplet collisions occur upon the inter-injector spray impingement, Zhang et al.'s model predicts smaller SMR and larger N_p than does the O'Rourke's model because the former tends to predict droplet bouncing while the latter tends to predict droplet coalescence. In the swirl case, the differences between the two model predictions are however not as significant as those in the non-swirl case. The explanation is that droplet collisions are not comparably frequent upon the

intra-injector spray interaction, which is induced by the swirling flow around the sprays. Consequently, increasing the swirling intensity or reducing the injection pressure may enhance the intra-jector spray interaction. Compared with the O'Rourke's model, Zhang et al.'s model predicts slightly higher A_d after -3° ADTC, which however results in indistinguishable premixed fuel mass. Because of the absence of fuel consumption by combustion, the premixed fuel mass accumulated in the gas-phase monotonically increase with time.

To substantiate a speculation that the rapid fuel vaporization and combustion in the reacting combustion may have significant influence on the interaction of sprays, we repeated the simulations in Figures 8 and 9 but under a reacting flow condition. It is interestingly seen that neither inter-injector nor intra-injector spray interactions appear to be noticeable when combustion happens. The substantially enhanced droplet vaporization under high temperature makes the droplets disappear before they could come to collide with each other. Although Figure 11 (d) shows a trace of intra-injector spray interaction with the presence of swirl, such a weak interaction is unlikely to effect frequent droplet collisions and therefore affect the spray characteristics. Because of the lack of frequent droplet collisions under combustion condition, both droplet collision models predict almost the same trends for all the quantities characterizing the sprays and combustion, as shown in Figure 12. The slight differences between the models in predicting N_p and hence A_d do not cause any noticeable changes on the predictions of heat release rates and cylinder pressure. We further noted that, compared with the case shown in Figure 8, the higher engine speed of 2000 rpm leaves significantly less time for droplet interaction in the combustion cylinder. It may be concluded that droplet collision would play a more important role under lower engine speed and high load conditions.

As discussed in Section 3, the TAB model implemented in the original KIVA 3V code was adopted in the present study for modelling droplet breakup. The excessive atomization predicted by the TAB model will produce smaller droplets with smaller inertia and hence smaller penetration depths before they are completely vaporized and burned out. Consequently, we expect that the spray impingement will be enhanced in OPCI and therefore the role of droplet collision will be more noticeable if other droplet breakup model, such as the KH-RT model, is adopted in the present calculation. Such a calculation focusing on the influence of droplet breakup on the present problem is certainly merited and will be considered in our future study.

4.3 Influence of Spray Layouts on Spray and Combustion Characteristics

As discussed in the Section 2, the spray layout used in the present experiment, as shown in Figure 3(a), is a specific variant of the more general Hofbauer's spray layout, as shown in Figure 3(b), for their six sprays nearly "crouch" on the Z=0 plane. We therefore proposed a new spray layout in the present study, as shown in Figure 3(c), in hope for fully utilizing the space in the combustion chamber for presumably better atomization and combustion. The new spray layout differs from the Hofbauer's in that the former has the S_2 symmetry with respect to the Z=0 axis while the latter has the C_2 symmetry to the same axis. It is expected that the present layout has more distributed sprays and droplets for enhancing fuel vaporization and mixing with air, which may result in enhanced combustion performance. As we have showed in the preceding subsection, the inter-injector spray impingement is unlikely under the combustion condition of high engine speed and low load. The intra-injector spray interaction is believed to be suppressed

in the present layout because of the distributed sprays. Consequently, droplet collisions will be less frequent in the present spray layout compared with the Hofbauer's layout.

To quantify the difference of these two spray layouts in affecting the spray and combustion characteristics, we compared the simulation results under two different engine speeds but the same 75% load. Figure 13 (a)-(c) illustrate the results for the case of engine speed of 1500 rpm, in which SOI= -5° ATDC and EOI =10° ATDC; Figure (d)-(f) illustrate the results for the case of engine speed of 2000 rpm, with SOI=-5° ATDC and EOI=15° ATDC.

For both layouts and for the engine speed of 1500 rpm and 75% load, SMR decreases rapidly after the fuel injection at -5 ATDC and then reaches a value of approximately 60 μm. Because the IT (around -2° ATDC) in the Hofbauer's layout is earlier than that (around TDC) in the present layout, as seen in the Figure 13 (c), the earlier temperature increase and fuel droplet evaporation in the Hofbauer's layout results in slightly smaller SMR and larger N_p than those in the present layout. By the same token, the present layout produces a significant higher N_p, A_d and the premixed fuel mass after -2° ATDC, when ignition occurs in the Hofbauer's layout, as shown in Figure 13 (b).

Figure-13 (c) shows the influence of spray layout on the heat release rate (on the left Y-axis) and cylinder pressure (on the right Y-axis). The earlier ignition in the Hofbauer's layout may be attributed to that the layout produces a higher mixture formation rate in the early stage. This can be further substantiated by observing the spatial distributions of fuel mass fraction and temperature at -2° ATDC, as shown in Figure 14. It is seen that a richer mixture area can be found in the Hofbauer's layout and therefore leads to a higher temperature kernel indicating the

occurrence of ignition. Owing to its later ignition, the present layout produces more mixture in the ignition delay period, which in turn causes intense combustion and a higher peak value of heat release rate. In terms of the cylinder pressure, there is no significant difference between the predictions of two spray layouts, regardless of some small discrepancies in the earlier stage.

Figures 12 (d)-(f) extend the above comparison to a higher engine speed of 2000 rpm. It is seen that the present layout predicts slightly smaller SMR while higher N_p, resulting in the almost very similar A_d and premixed fuel mass as shown in Figure 13 (e). Due to the small difference of the spray characteristics, there is no significant difference for the predicted heat release and cylinder pressure between the Hofbauer's layout and the present one. These observations are consistent with the preceding conclusion that the high-speed engine operation results in almost instantaneous ignition, as shown in Figure 13 (f), which leaves no time for the spray development and therefore cannot differentiate the two spray layouts.

Different spray angles such as α, β and γ may influence the spray and combustion characteristics. Figure 15 show the effects of different α β and γ on the the heat release rate in the present layout and the Hofbauer's layout. The condition of the engine speed of 1500 rpm and 75% load was used because it can maximize the difference between the two layouts. Several interesting observations can be made as follows. First, both layouts show slight dependence on α varying from 10° to 40°. This can be understood by noting that α measures the deviation of No. 1 (or No. 3, No. 4, No. 6 by symmetry) spray from the Y-axis on the Z=0 plane, and that the larger α the wider spreading of the sprays to the combustor periphery. Unless the wall-impingement occurs at sufficiently large α, say α =50°, increasing α can facilitate uniform fuel distribution in

the combustion chamber and enhance combustion heat release. However, the earlier ignition and shorter ignition delay with increasing α makes a longer period of time for mixture formation which in turn causes lower peak value of heat release rate. This argument can possibly explain the peak values of the heat release rate non-monotonically change with increasing α from 10° to 40°.

The second observation is that varying β from 0° to 12° has negligible influence on the present layout although it has significant effects in the Hofbauer's layout. In the Hofbauer's layout, β measures the deviation of the in-plane No. 2 (or No. 5 by symmetry) spray from the Y-axis on the Z=0 plane; increasing β bring No. 2 spray closer to No. 1 spray and therefore enhance their interaction. In the present layout, No. 2 spray lays on the different side of the Z=0 plane from No. 1 and 3 sprays so that the slight variation of β from 0° to 12° makes insignificant change to the spatial distribution of the sprays. It should be noted that further increasing β may cause the impingement of No. 2 spray on the bottom wall and hence should be avoided in the layout design.

The third observation is again the moderate dependence of the heat release rate on γ varying from 0° to 12°. The increase of γ deviates the "side" sprays (i.e. No. 1, 3 and 4, 6) from the "central" sprays (i.e. No. 2 and 5) and consequently enhance the spray spreading in the combustion chamber. Similar to the limitation on the variation of β, γ cannot be too large or the "side" sprays may impinge the combustion chamber edge.

5. Concluding Remarks

An experimental and computational investigation of spray impingement and combustion in a model OPCI engine was conducted to extend the authors' previous study of non-reacting spray impingement to realistic OPCI operating conditions, with the following particular research focuses.

The first focus of the study is to clarify the important role of droplet collision, particularly droplet bouncing, in modeling impinging spray combustion under the OPCI engine conditions. A recently proposed (Zhang et al., 2016) pressure-dependent droplet collision model was implemented in the KIVA-3V computer program to simulate complete engine cycles of the OPCI engine. The practical and simple model was established by correcting the deficiency of the O'Rourke's model in overlooking the phenomenon of droplet bouncing, by modifying the Estrade et al.'s model to account for the increasing propensity of droplet bouncing at high pressures, and by being validated against the previous experiments on non-reacting spray impingement. The present results show that, compared with the widely-used O'Rourke's model, the present model is believed to make more physically reliable predictions when droplet collisions become more frequent in the combustion chamber at high engine pressures.

The second focus of the study is to determine the possible enhancement or suppression mechanisms of droplet collision through the spray impingement (or interaction in general) in the OPCI engine by rapid droplet vaporization and combustion, varying the engine speed or load, and introducing in-cylinder swirling flow. The results show that inter-injector spray impingement

can be observed under non-reacting condition but it is absent under the reacting condition because the penetration lengths of droplets are shortened by their rapid vaporization at high temperatures. Increasing the engine speed will promote the engine combustion and hence suppress the inter-injector spray impingement, while increasing the engine load will produce denser sprays containing more droplets and hence enhance the spray impingement. Introducing in-cylinder swirl to the combustion chamber has a dual effect on the spray impingement: it deflects the sprays from being impinged, but it however promotes intra-injector spray interaction, given the injector geometry allows.

The final focus of the study is to explore the possible advantages of a newly proposed spray layout that has the S_2 symmetry to utilize the space of combustion chamber. By comparing it with the Hofbauer's layout possessing the C_2 symmetry, the new layout is found to produce more distributed premixed fuel mass and hence to result in a longer ignition delay time but a higher peak heat release rate. Computationally parametric study of three geometric angles, which can completely define the present and the Hofbauer's layouts, has been conducted for their influence on the heat release rate. Further geometric optimization of the OPCI engine, comprehensive and advanced experimental verification, and LES with more sophisticated models for turbulence, droplet breakup and vaporization are still merited for future studies.

Acknowledgments

The authors are grateful for the generous support and valuable advice of Prof. Changlu Zhao and Prof. Fujun Zhang for establishing the experimental setup.

Funding

The work was supported by the Hong Kong Research Grants Council/General Research Fund (PolyU 152217/14E and PolyU 152651/16E) and in part by the Hong Kong Polytechnic University (operating under Contract Nos. G-UA2M and G-UBGA).

Reference

Amsden, A. A. 1997. KIVA-3V: A block-structured KIVA program for engines with vertical or canted valves, Los Alamos National Lab., NM (United States).

Aumann, R., McCracken, M. and Abraham, J. 2002. An evaluation of a composite model for predicting drop-drop collision outcomes in multidimensional spray computations, SAE Technical Paper.

Brazier-Smith, P., Jennings, S. and Latham, J. 1972. The interaction of falling water drops: coalescence. Proc. Royal Society of London A: Math, Phy and Eng Sci, ***326****(1566), 393-408.*

Chiba, T., Saito, M., Amagai, K. and Arai, M. 2000. Inter-spray impingement of two diesel sprays. Proc. Int. Conf. Liquid Atomization and Spray Systems (ICLASS) (pp. 16-20).

Estrade, J.-P., Carentz, H., Lavergne, G. and Biscos, Y. 1999. Experimental investigation of dynamic binary collision of ethanol droplets–a model for droplet coalescence and bouncing. International Journal of Heat and Fluid Flow, ***20****(5), 486-491.*

Franke, M., Huang, H., Liu, J. P., Geistert, A. and Adomeit, P. 2006. Opposed Piston Opposed Cylinder (opoc™) 450 hp Engine: Performance Development by CAE Simulations and Testing,

SAE Technical Paper.

Heywood, J. B. 1988. Internal combustion engine fundamentals. Mcgraw-hill New York.

Hofbauer, P. 2005. Opposed piston opposed cylinder (opoc) engine for military ground vehicles, SAE Technical Paper.

Huo, M., Huang, Y. and Hofbauer, P. 2015. Piston Design Impact on the Scavenging and Combustion in an Opposed-Piston, Opposed-Cylinder (OPOC) Two-Stroke Engine, SAE Paper 2015-01-1269.

Jiang, Y., Umemura, A. and Law, C. 1992. An experimental investigation on the collision behaviour of hydrocarbon droplets. J. Fluid Mech, ***234****, 171-190.*

Kim, S., Lee, D. J. and Lee, C. S. 2009. Modeling of binary droplet collisions for application to inter-impingement sprays. Int. J. Multiphase Flow, ***35****(6), 533-549.*

Krieger, R. and Borman, G. L. 1967. Computation of apparent heat release for internal combustion engines. Mech Eng, ***89****(1), 59-70.*

Launder, B. E. and Spalding, D. B. 1972. Lectures in mathematical models of turbulence.

Law, C. K. 2010. Combustion physics. Cambridge university press.

Maruyama, Y. and Saito, M. 2001. Effect of Inter-Impingement Process on the Behavior of a Diesel Spray. In: Proc. ILASS-Asia, ***2001****, 241-246.*

Munnannur, A. 2007. Droplet Collision Modeling in Multi-dimensional Engine Spray Computation, University of Wisconsin-Madison.

Munnannur, A. and Reitz, R. D. 2007. A new predictive model for fragmenting and

non-fragmenting binary droplet collisions. International journal of multiphase flow, ***33****(8), 873-896.*

Naik, S., Johnson, D., Koszewnik, J., Fromm, L., Redon, F., Regner, G. and Fuqua, K. 2013. Practical applications of opposed-piston engine technology to reduce fuel consumption and emissions, SAE Technical Paper.

O'Rourke, P. J. 1981. Collective drop effects on vaporizing liquid sprays (No. LA-9069-T), Los Alamos National Lab., NM (USA).

O'Rourke, P. J. and Amsden, A. A. 1987. The TAB method for numerical calculation of spray droplet breakup, Los Alamos National Lab., NM (USA).

Pirault, J.-P. and Flint, M. 2010. Opposed Piston Engines: Evolution, Use, and Future Applications. SAE international.

Qian, J. and Law, C. 1997. Regimes of coalescence and separation in droplet collision. Journal of Fluid Mechanics, ***331****, 59-80.*

Redon, F., Kalebjian, C., Kessler, J., Rakovec, N., Headley, J., Regner, G. and Koszewnik, J. 2014. Meeting Stringent 2025 Emissions and Fuel Efficiency Regulations with an Opposed-Piston, Light-Duty Diesel Engine, SAE Paper 2014-01-1187.

Regner, G., Herold, R. E., Wahl, M. H., Dion, E., Redon, F., Johnson, D., Callahan, B. J. and McIntyre, S. 2011. The Achates Power Opposed-Piston Two-Stroke Engine: Performance and Emissions Results in a Medium-Duty Application, SAE Paper 2011-01-2221.

Sirignano, W. A. 1999. Fluid dynamics and transport of droplets and sprays. Cambridge

University Press.

Tang, C., Zhang, P. and Law, C. K. 2012. Bouncing, coalescence, and separation in head-on collision of unequal-size droplets. Physics of Fluids (1994-present), ***24****(2), 022101.*

Tennison, P. J., Georjon, T. L., Farrell, P. V. and Reitz, R. D. 1998. An experimental and numerical study of sprays from a common rail injection system for use in an HSDI diesel engine, SAE Technical Paper.

Venugopal, R., Abani, N. and MacKenzie, R. 2013. Effects of Injection Pattern Design on Piston Thermal Management in an Opposed-Piston Two-Stroke Engine, SAE Paper 2013-01-2423.

Zhang, P. and Law, C. K. 2011. An analysis of head-on droplet collision with large deformation in gaseous medium. Physics of Fluids, ***23****(4), 042102.*

Zhang, Z., Chi, Y., Shang, L., Zhang, P. and Zhao, Z. 2016. On the role of droplet bouncing in modeling impinging sprays under elevated pressures. Int. J. Heat Mass Transfer, ***102****, 657-668.*

Zhao, Z., Wu, D., Zhang, F. and Zhang, Z. 2014. Design and Performance Simulation of Opposed-Piston Folded-Cranktrain Engines, SAE Paper 2014-01-1638.

Figure 1. Schematic of the model OPCI engine for (a) gas exchange and (b) fuel injection and multiple spray impingement.

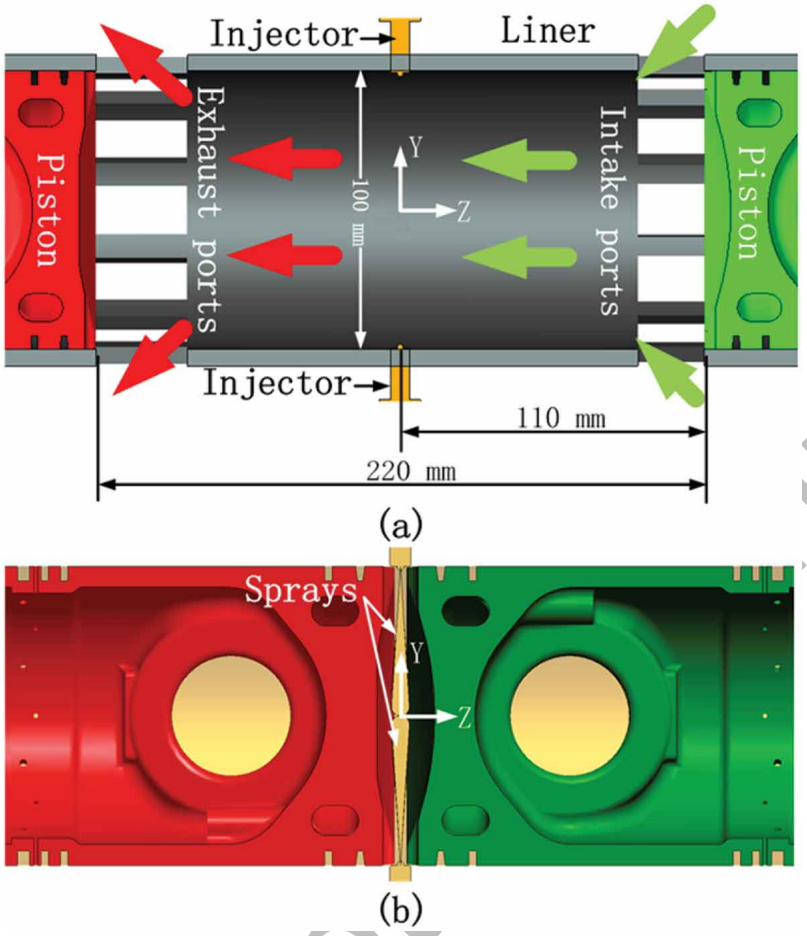

Figure 2. Schematic of test system for the model OPCI engine. (1) Engine prototype, (2) Electrical dynamometer, (3) Engine load cell, (4) Fuel tank, (5) Fuel injectors, (6) Electronic scale, (7) Cylinder pressure transducer, (8) Crank angle sensor, (9) Intake pressure transducer, (10) Exhaust pressure transducer, (11) Fuel oil driving pressure sensor, (12) Common rail, (13) Intake temperature sensor, (14) Exhaust temperature sensor, (15) Charge amplifier. (16) Data collection system.

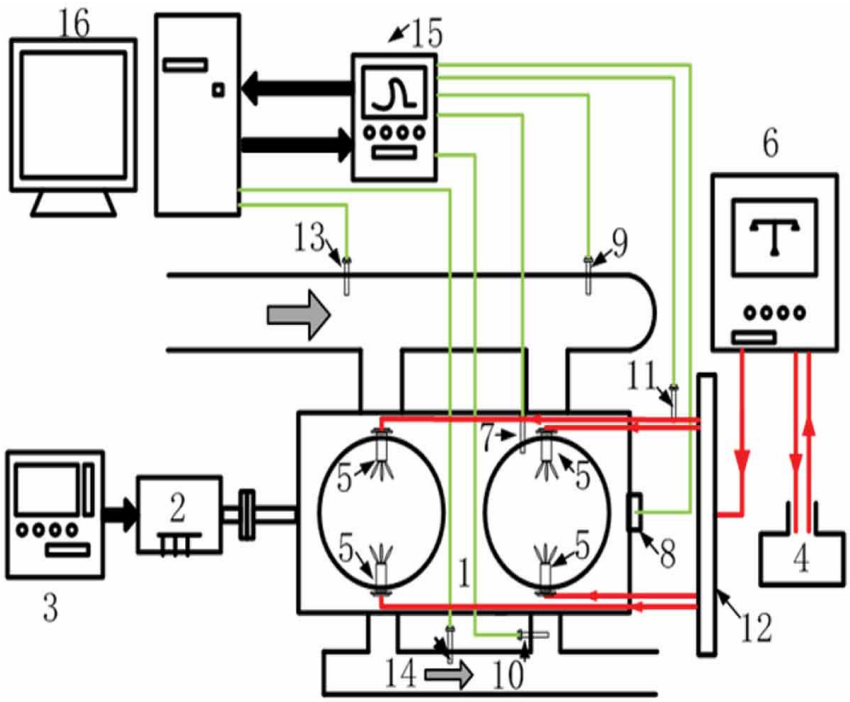

Figure 3. Schematic of fuel spray layouts in the model OPCI. (a) the spray layout used in the present experiment, (b) Hofbauer's sprays layout and (c) the spray layout used in the present simulation. The projections of each layout to the planes of X=0, Z=0 and Y=0 are from left to right, respectively.

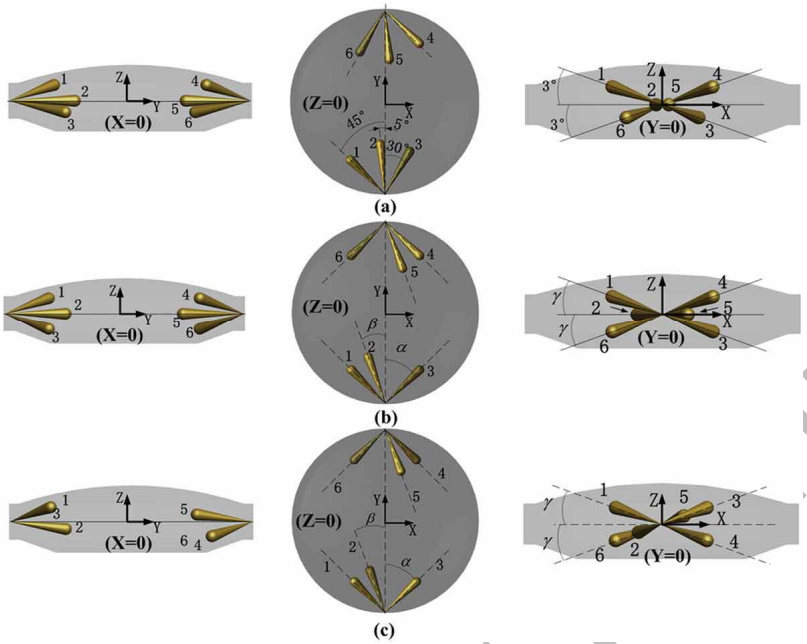

Figure 4. Regime nomograms of droplet collision used for establishing (a) O'Rourke's model and (b) Zhang et al.'s model.

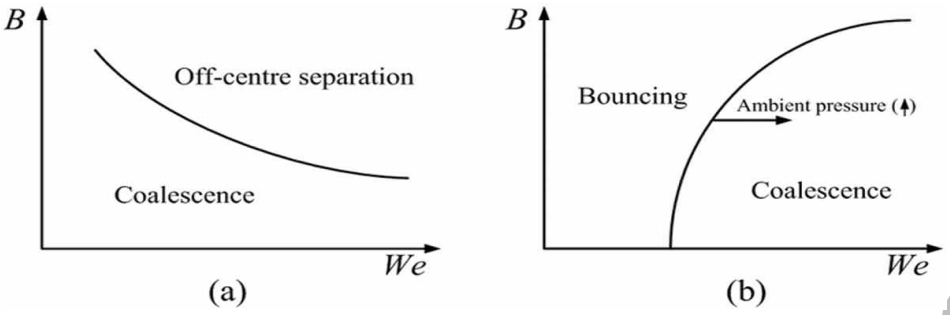

Figure 5. Dynamical mesh of the model OPCI engine at (a) Bottom Dead Center (BDC) (the number of cells is 200615) and (b) Top Dead Center (TDC) (the number of cells is 32748).

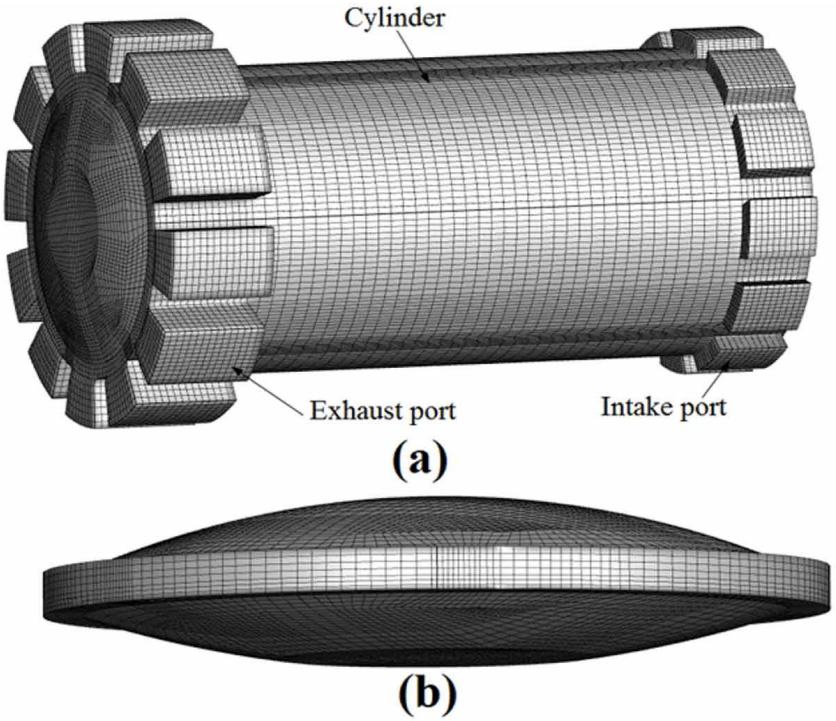

Figure 6. Mesh dependence of the calculated cylinder pressure in the model OPCI engine.

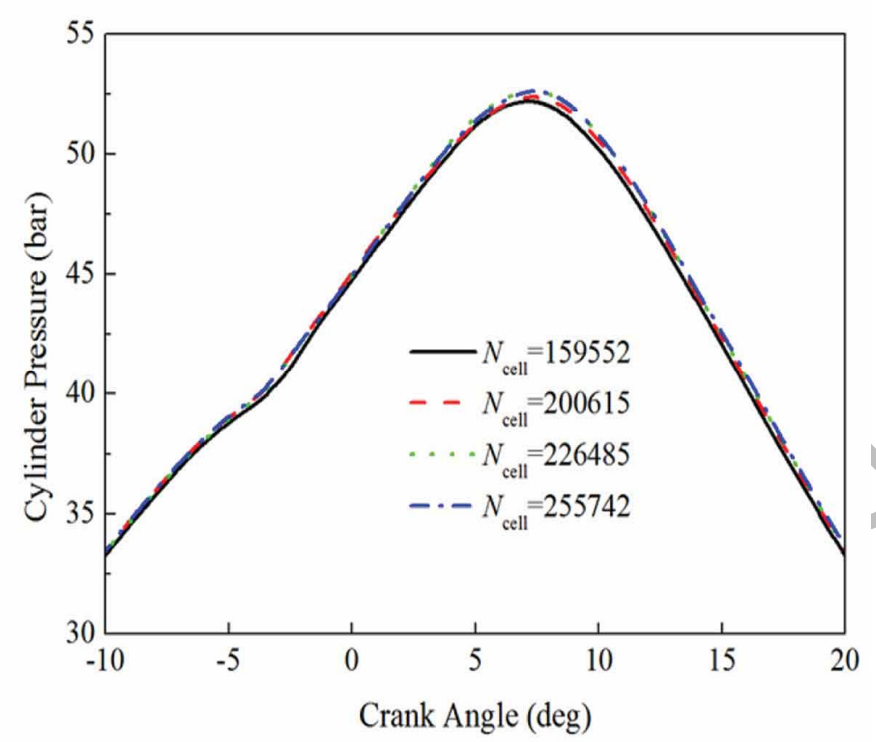

Figure 7. Cylinder pressure (on the left Y-axis) and heat release rate (on the right Y-axis) under the conditions of (a) 1500rpm 50% load and (b) 2000rpm 50% load.

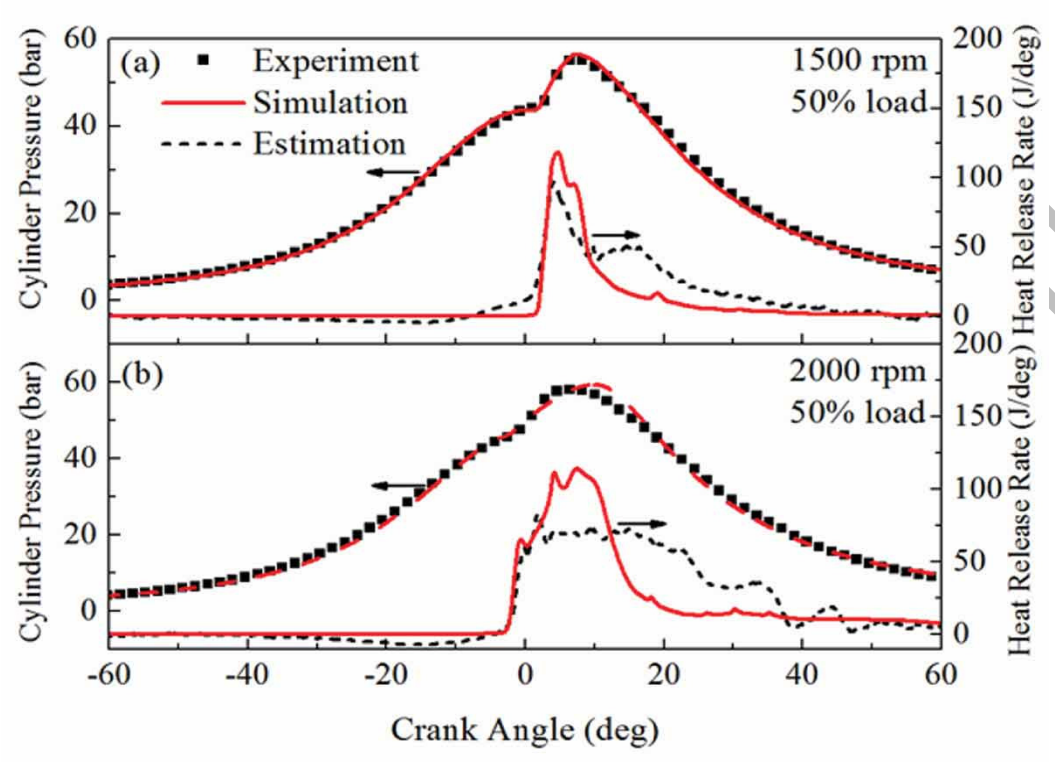

Figure 8. Comparison between Zhang et al.'s and O'Rourke's models for predicting the characteristics of impinging spray combustion in the model OPCI engine under the engine speed of 1500 rpm, and(a)-(c) 50% load ; (d)-(f) 75% load. (a) and (d) SMR (on the left Y-axis) and N_p (on the right Y-axis); (b) and (e) A_d (on the left Y-axis) and total mass of premixed fuel (on the right Y-axis); (c) and (f) the heat release rate (on the left Y-axis) and the average cylinder pressure (on the right Y-axis). The ignition times denoted by IT are indicated in (c) and (f).

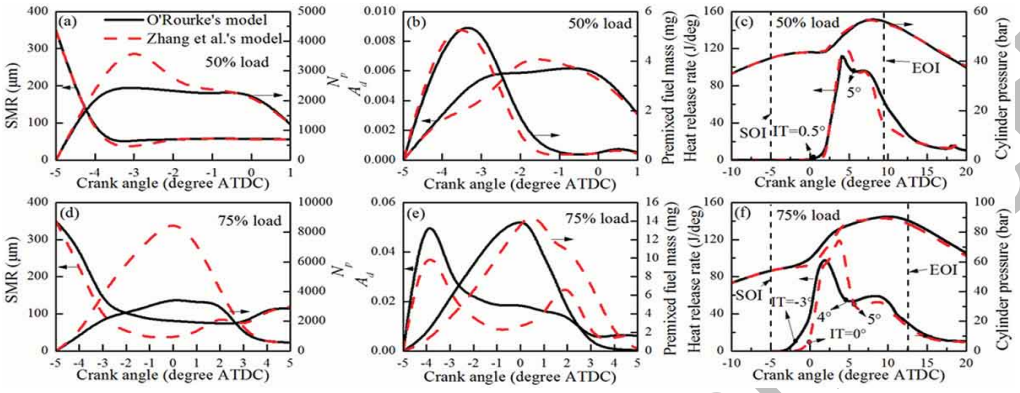

Figure 9. Non-reacting spray evolution and interaction under the non-swirl and swirl conditions, predicted by O'Rourke's model in (a) and (c) and Zhang et al.'s model in (b) and (d). The engine speed is 2000rpm and the load 75%.

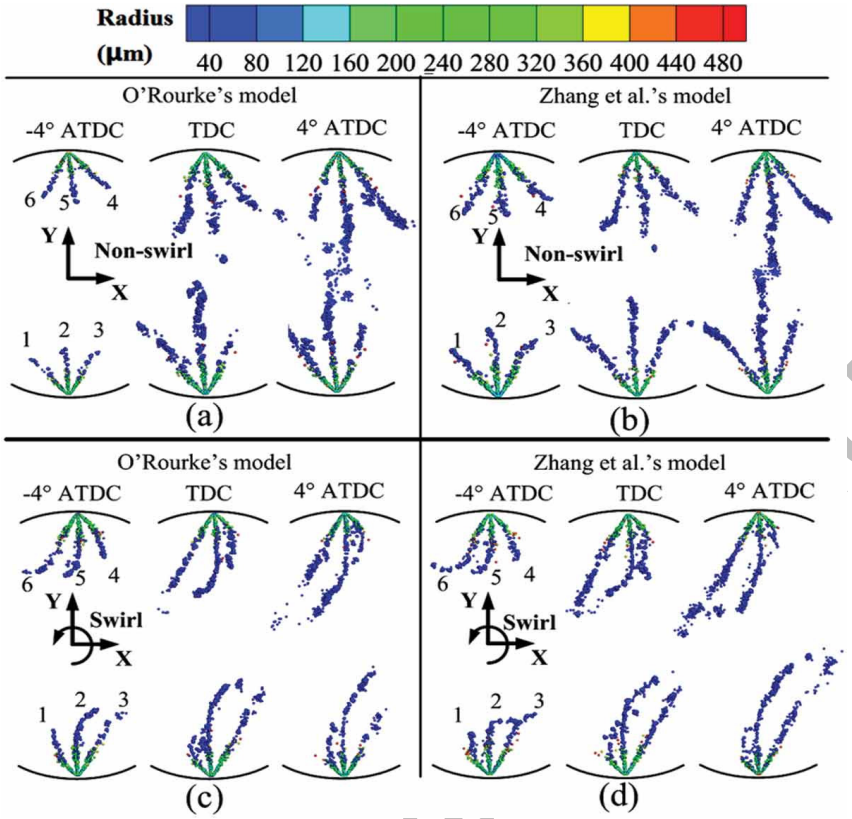

Figure 10. Quantitative comparison between the O'Rourke's model and Zhang et al.'s model under non-swirl [shown in (a) and (b)] and swirl [shown in (c) and (d)] conditions for predicting the non-reacting spray characteristics illustrated in Figure 8. (a) and (c) the overall SMR (on the left Y-axis) and N_p (on the right Y-axis); (b) and (d) A_d (on the left Y-axis) and total mass of pre-mixed fuel on (right the Y-axis).

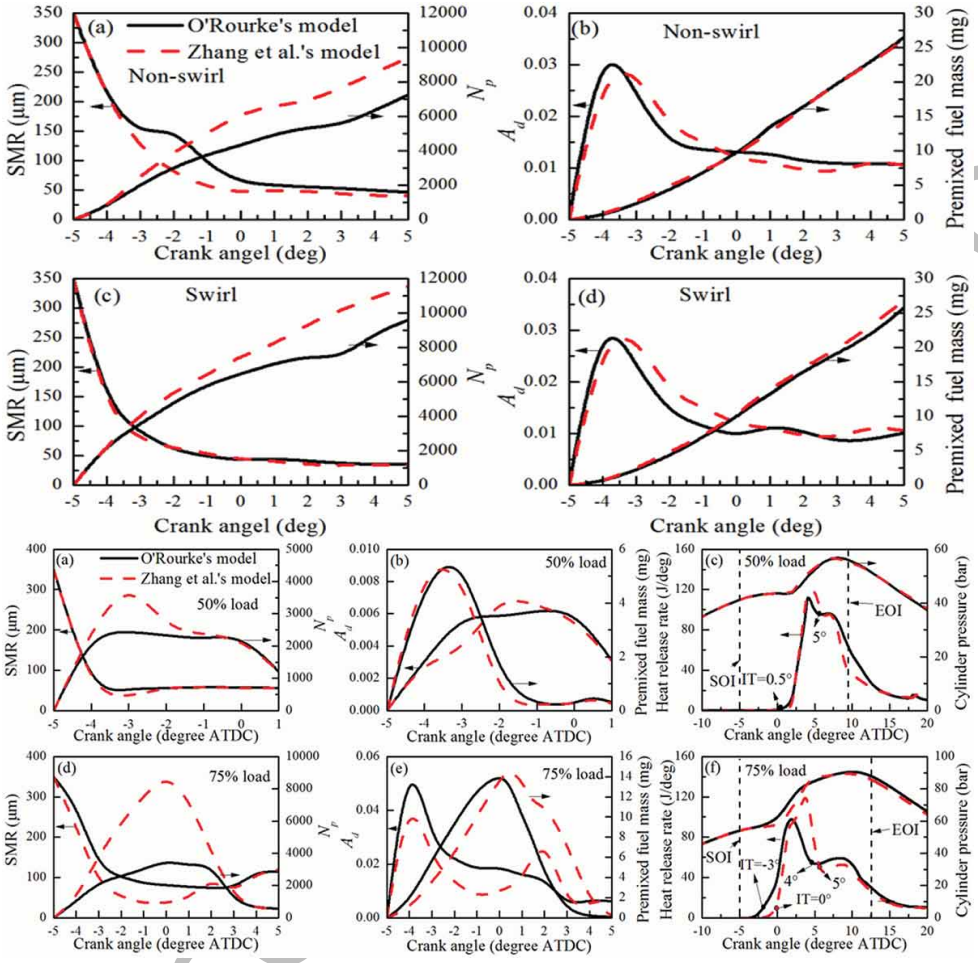

Figure 11. Evolution of reacting sprays under non-swirl and swirl conditions, predicted by O'Rourke's model in (a) and (c) and by zhang et al.'s model in (b) and (d). The engine speed is 2000rpm and the load 75%.

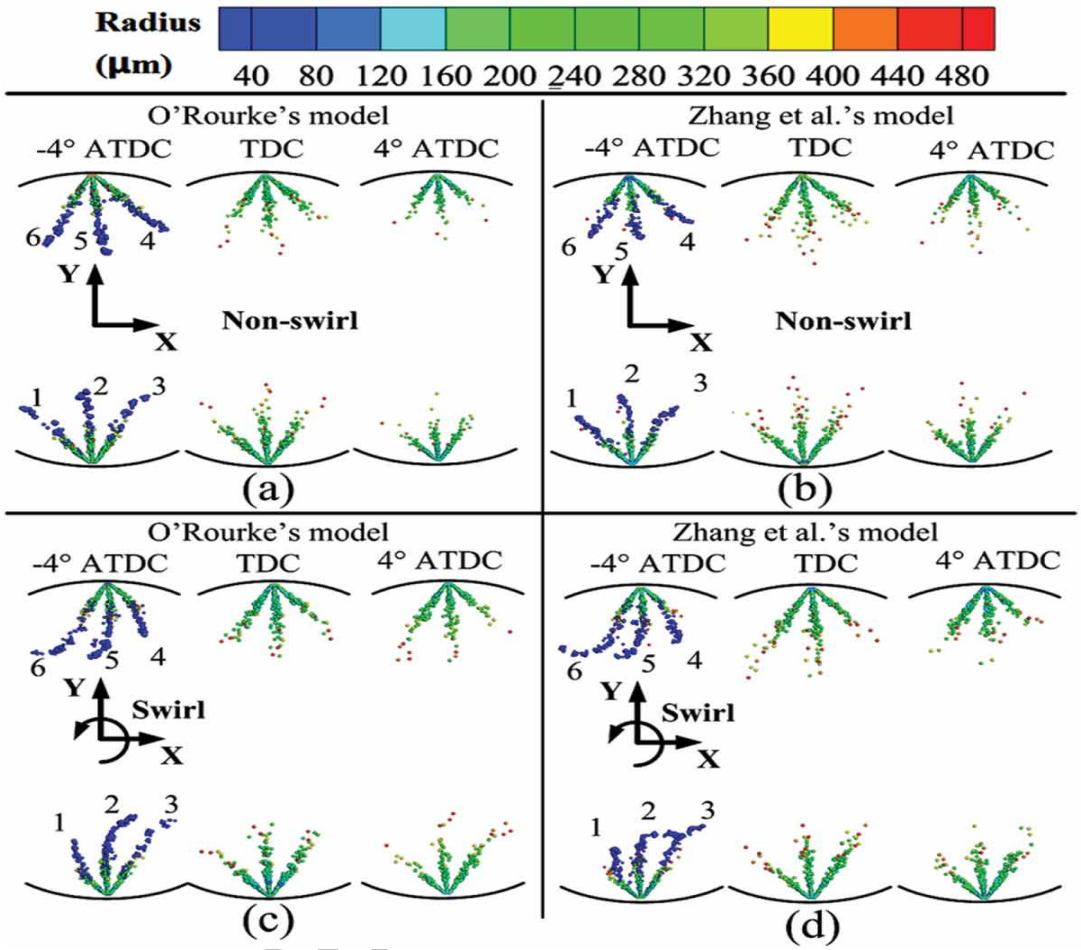

Figure 12. Quantitative comparison between the O'Rourke's model and Zhang et al.'s model under non-swirl [shown in (a)-(c)] and swirl [shown in (d)-(f)] condictions for predicting the spray impingment and combustion at the engine speed of 2000 rpm under 75% load. (a) and (d) the overall SMR (on the left Y-axis) and N_p (on the right Y-axis); (b) and (e) A_d (on the left Y-axis) and total mass of pre-mixed fuel on (right the Y-axis); (c) and (f) the heat release rate (on the left Y-axis) and the average cylinder pressure (on the right Y-axis).

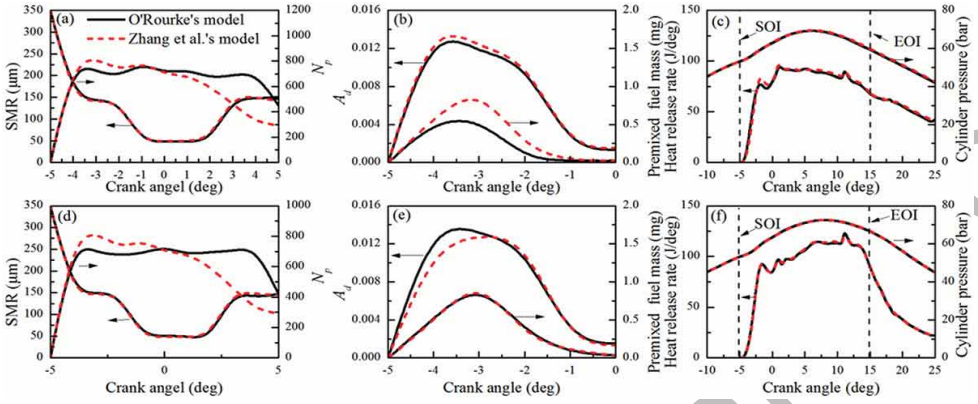

Figure 13. Comparison between present layout and Hofbauer's layout predicting the impinging spray combustion characteristics in the model OPCI engine under the engine speed of 1500rpm 75% load, shown in (a)-(c), and 2000 rpm 75 % load, shown in (d)-(f). (a) and (d) the overall SMR (on the left Y-axis) and N_p (on the right Y-axis); (b) and (e) A_d (on the left Y-axis) and total mass of pre-mixed fuel on (right the Y-axis); (c) and (f) the heat release rate (on the left Y-axis) and the average cylinder pressure (on the right Y-axis).

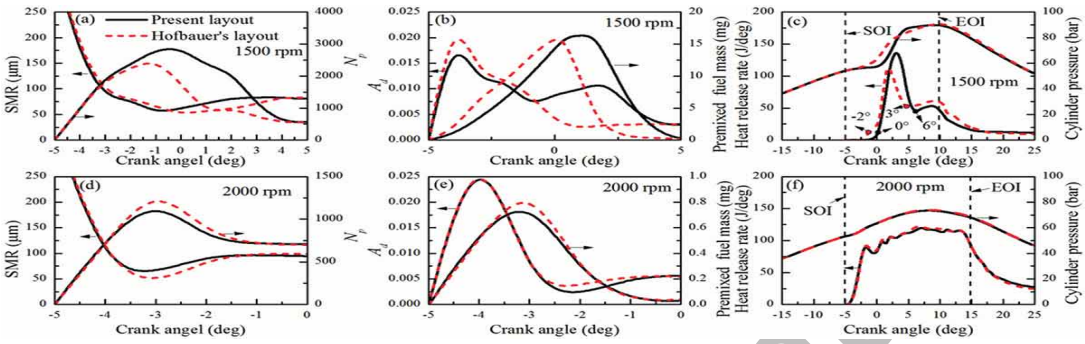

Figure 14. Fuel mass fraction (on the left) and temperature (on the right) for (a) the Hofbauer's layout and (b) the present layout on Y=-4 cm, -3 cm, -1.5 cm, 0 cm, 1.5 cm, 3 cm and 4 cm planes (from left to right) at -2 °ATDC. The translucent shade is the combustion chamber edge.

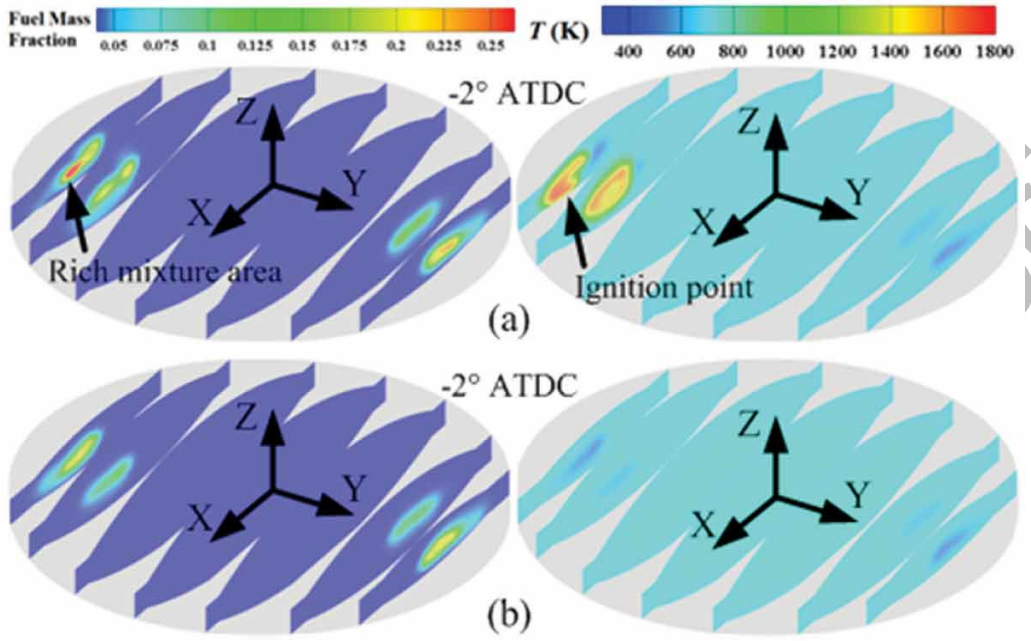

Figure 15. Evolution of heat release rate for the present layout [shown in (a)-(c)] and the O'Rourke's layout [shown in (d)-(f)] with various α, β and γ. (a) and (d) show the influence of variable α; (b) and (e) β; (c) and (f) γ. The engine speed is 1500 rpm and the load 75%.